Zonal Isolation Material for Low-Temperature Shallow-Depth Application: Evaluation of Early Properties Development

Madhan Nur Agista[1]*, Mahmoud Khalifeh[1], Arild Saasen[1], and Elakneswaran Yogarajah[2]

[1]University of Stavanger
[2]Hokkaido University

Summary

Shallow-depth cementing presents unique challenges due to its low temperature and low pore pressure characteristic. The curing process of the cementitious material is typically prolonged at low temperatures resulting in a delayed curing process. The use of a low-density slurry to mitigate low pore pressure introduces another challenge, as it leads to a reduction in the final compressive strength. On the other hand, the operation requires the material to develop enough strength swiftly to be able to efficiently continue the next drilling operation. In addition, the presence of flow zones such as shallow gas and shallow water flow increases the complexity of the cementing process. There have been many developments in cementitious materials for shallow-depth cementing such as rapid-hardening cement and gas tight cement. However, there is little research focusing on the performance evaluation of each material at low-temperature conditions. This paper aims to present a thorough material evaluation for low-temperature shallow-depth cementing. The incorporated materials are American Petroleum Institute (API) Class G cement, rapid-hardening cement, gas tight cement, and geopolymer. Geopolymer is included to evaluate its potential as the green alternative to Portland-based cement. The sets of characterization were conducted during the liquid, gel, and solid phases. The samples were prepared under wide-ranging low temperatures and typical bottomhole pressures for shallow sections. The result shows different performances of each material and its behavior under low temperatures such as prolonged strength development and low reactivity, which necessitates further development of these materials.

Introduction

Effective zonal isolation of oil and gas wells is crucial to the overall success of well construction and production. In the North Sea region, shallow depth presents unique challenges for zonal isolation. Low-temperature conditions are prevalent in these shallow depths, which can cause traditional cementing materials to fail, leading to the loss of zonal isolation. The surface casing cementing process requires cement to be placed all the way to the seabed, which exposes it to seabed temperatures reaching to 4°C. Low temperatures can significantly affect the performance of the cement, leading to several issues, such as reduced strength and increased setting time. A previous study by Agista et al. (2022a) shows prolonged curing time and static gel strength development of cementitious materials at low temperatures. In this case, having enough compressive strength at low temperatures after a short curing time is necessary to have confidence in continuing the drilling process for the following casing sections. Other challenges on the shallow depth are the relatively low pore pressure and weak unconsolidated behavior of the formation that increases the complexity of proper zonal isolation material design. To address this, low-density cementitious material through water-extended, foamed, or lightweight aggregates is required (Nelson and Guillot 2006). However, the lower final compressive strength of low-density cement is a concern, especially in environments with low temperatures, as it may affect the long-term integrity of the wellbore (Rae and Di Lullo 2004). In addition, the presence of flow zones such as shallow gas and water flow further complicates the cementing process, potentially compromising its effectiveness and leading to costly failures with significant environmental and safety implications.

There have been some reports on the failures of zonal isolation, particularly at shallow depths, underlining the importance of effective zonal isolation design and implementation. Vielstädte et al. (2017) reported methane gas leakage from three decommissioned wells in the central North Sea from shallow depth. Hydroacoustic surveys by Böttner et al. (2020) found that 28 out of 43 decommissioned wells in similar areas released gas from the seafloor. The source of the gas leakage was identified from shallow gas zones at a depth of 400 to 800 m through sonar survey, gas sampling, operation records, and seismic interpretation. These leakages from abandoned wells confirm the catastrophic results of well integrity failures (Bachu 2017; Wilpshaar et al. 2021). In another case study, Tveit et al. (2021) found significant rates of gas dissolution in seawater and release into the atmosphere from 20 wells that underwent plug and abandonment, highlighting the importance of proper zonal isolation. In some cases (for example, in deep water where gas hydrates are present on the seabed), cement hydration can increase methane leaks due to an exothermic reaction that melts the hydrates and releases methane gases. Therefore, the presence of hydrates will not be considered in our case study. Selecting suitable materials for zonal isolation is crucial to prevent such leakages and ensure long-term zonal isolation.

Various types of cementitious materials for low-temperature shallow-depth cementing applications have been developed and widely used, such as rapid-hardening cement (Bensted 1991) and gas tight cement (Grinrod et al. 1988). Recent development shows a positive result of adding inorganic salt for improving setting time and early compressive strength at low temperatures (Xu et al. 2023). In this paper, the performance of the mentioned materials, including an API Class G cement and a granite-based geopolymer, is compared. The evaluation will be based on critical properties, such as viscous properties, pumpability, static fluid loss, static gel strength, and

*Corresponding author; email: madhan.n.agista@uis.no

Original SPE manuscript received for review 7 June 2023. Revised manuscript received for review 10 July 2023. Paper (SPE 217434) peer approved 11 July 2023.

compressive strength, which all are essential for effective zonal isolation. Characterization techniques such as X-ray diffraction (XRD) and particle-size distribution (PSD) are used to understand the behavior of the materials better. By comparing and evaluating these materials, this paper aims to provide insights into their effectiveness and suitability for use in low-temperature shallow-depth wells. The results reveal the important parameters which could be improved and further developed and can help guide the selection of appropriate materials for zonal isolation, improve wellbore stability, ensure well integrity, and optimize production in this uniquely challenging environment, low-temperature shallow-depth.

Cementitious Material. Zonal isolation materials for well cementing must meet certain criteria to minimize the risk of uncontrolled flow during well construction and production operations and to control the potential risk of flow zones such as shallow water and gas flows (NORSOK Standard D-010 2013). The development of API Class C cement has opened up the possibility for efficient surface casing/liner cementing jobs at low-temperature shallow-depth zones by increasing reactivity through particle size and higher alumina content for early strength development. However, in some cases, Class G cement is still used in surface casing cementing operations, mostly as tail cement. As a green alternative, geopolymer has shown the potential to be used as a zonal isolation material, though investigations for low-temperature shallow-depth cementing are to some degree limited. Therefore, four different materials were evaluated in-depth for their performance.

Neat G Cement. Neat G cement, an API Class G Portland cement, is widely used for well construction and plug and abandonment applications due to its well-understood performance, affordability, and availability (Nelson and Guillot 2006). The performance of neat G is limited due to the difference in cementing sections with wide-ranging pressure and temperature. For shallow-depth cementing, neat G is not ideal due to its high density and inability to handle low temperatures due to prolonged hydration. Al Ramadan et al. (2019) performed an annular gas migration test using neat G and concluded that it does not have any ability to serve as a primary barrier in the wellbore annulus without any additives. The cement used in the experiment was manufactured by Dyckerhoff and prepared following the API 10B-2 standard with only distilled water of 44 wt% (API RP 10B-2 2013).

Rapid-Hardening Cement. This type of cement is equivalent to API Class C, which is widely used for shallow-depth cementing. Thus, it is named API Class C cement in this paper. Meanwhile, rapid-hardening cement refers to the mixture of API Class C cement mixed with extender and other additives. API Class C cement has a smaller particle size and relatively higher tricalcium aluminate (C_3A) content compared with Class G cement (Nelson and Guillot 2006; Bensted 1991). Smaller particle size improves the reactivity of the material and enables a higher water-to-cement ratio to lower the slurry density. Rapid-hardening cement is typically used for shallow depths because it cures faster, reducing waiting time between drilling and increasing overall efficiency and profitability. Opseth et al. (2009) reported the successful cementing operation at 13 3/8-in. casing in the presence of shallow water flow using rapid-hardening cement. In this paper, rapid-hardening cement was used with the combination of a water-based extender with a total liquid-to-solid ratio of 85%. Artificial seawater is used as the main liquid phase. Seawater is believed to be able to increase early strength at low temperatures and reduce waiting-on-cement time for surface casing cementing (Smith and Calvert 1975). Moreover, seawater is safe and suitable to be used with other cement additives.

Gas-Tight Cement. Gas-tight properties were initially proposed as the solution to handle short-time gas migration with microsilica as the main additive on the mixture (Grinrod et al. 1988). Other materials, such as latex, were also tested for gas-handling applications (Drecq and Parcevaux 1988). Later, due to material safety, stability, and handling issues in the offshore rig, colloidal silica was proposed to replace microsilica in gas tight cement (Bjordal et al. 1993). Today, colloidal silica is one of the most used additives for gas tight cement for lightweight and annular gas-controlled cement. Colloidal silica can improve the early compressive strength of the cement at low temperatures by accelerating the formation of ettringite and producing more calcium silicate hydrate (C-S-H) gels (Bu et al. 2018). In this study, a mix of API Class C cement with colloidal silica additives is used, following the manufacturer's recommended liquid-to-solid ratio of 65%. Various additives, such as defoamers, fluid-loss additives, and retarders, are used to make the cement applicable for shallow-depth cementing.

Granite-Based Geopolymer. Geopolymer is defined as inorganic material rich in silica and alumina that will harden by a liquid hardener (Davidovits 2005). This material is categorized as hydraulic cementitious material, which behaves similarly to cement (pumpable and workable). However, unlike traditional cement, no hydration takes place during the reaction; instead, geopolymerization will take place initiated by a high alkalinity activator. Geopolymerization refers to the process of forming a hardened material, typically from sandstone or other silicate-based precursors, by using specific activators that start a chemical reaction leading to the formation of a geopolymer. The geopolymer precursor, which is the solid phase, may include low-calcium fly ash, thermally activated clay, or naturally occurring rocks (Khalifeh et al. 2019; Kamali et al. 2021). Meanwhile, the liquid phase is an alkali solution with a specified molar ratio. Geopolymerization involves three main mechanisms, which are dissolution of the aluminosilicate structure of the solid phase in the presence of hydroxyls, the orientation and reconnection of molecules due to an increase in the concentration of ions in the slurry, and the formation of oligomers followed by polycondensation by connecting oligomers and forming a long-chain structure of aluminosilicates (Davidovits 2020). The use of geopolymer for well cementing application has been growingly studied in recent years (Chamssine et al. 2021; Omran et al. 2022; Gomado et al. 2023). Moreover, the application of granite-based geopolymer for low-temperature cementing has recently been investigated and shows the ability to develop sufficient strength (Khalifeh et al. 2023). In this study, granite rock is normalized with blast furnace slag (BFS) and microsilica (see **Table 1**) and mixed with a potassium hydroxide solution to produce granite-based geopolymers. BFS is byproduct from iron production in a blast furnace and consists of silicate and aluminosilicates source. It has no cementitious ability by nature; however, it can be activated by lime, Portland cement, or alkali materials (Hewlett and Liska 2019). Microsilica is also added to increase the source of reactive amorphous silica with a high surface area to help early strength development.

Normalized Granite	SiO_2	Al_2O_3	Fe_2O_3	CaO	MgO	Na_2O	K_2O	TiO_2	MnO	SrO	BaO	S^{2-}	LOI	Total
wt%	62.51	9.92	0.43	16.06	5.78	1.78	1.81	1.02	0.01	0.01	0	0.58	0.13	100

Table 1—Geopolymer's solid precursor composition.

Experimental Methodology. The material is prepared following the recommendation from each manufacturer and according to the API standard (API RP 10B-2 2013). The cementitious material specification is presented in **Table 2.** To simulate downhole conditions, laboratory experiments were conducted under specific pressure and temperature conditions. The selected temperatures for surface casing

cementing were 4°C, 15°C, and 25°C, respectively, while the downhole pressure of 124 bar was used. The mixed slurries were conditioned using an atmospheric consistometer at 150 rev/min for 30 minutes at each specified temperature before performing all experiments as recommended by API RP 10B-2 (2013).

Cementitious Material	Solid Phase	Liquid Phase	Additives				
Neat G cement	Class G cement	Deionized water (44%)	–				
Rapid-hardening cement	Class C cement	Artificial seawater (85%)	Defoamer (0.01%)	Extender (1.0%)			
Gas-tight cement	Class C cement	Deionized water (65%)	Defoamer (0.1%)	Dispersant (1.7%)	Colloidal silica (7.3%)	Fluid loss (4.0%)	Retarder (1.8%)
Granite-based geopolymer	Normalized granite	Deionized water and KOH (44%)			–		

Table 2—Mixture of cementitious material used for the study.

Method

Particle-Size Distribution. PSD of cement significantly affects the hydration rate of the slurry. Cement with larger particle size tends to require more time to set and has delayed strength development compared with finer cement (Bentz et al. 1999). Therefore, for lower-temperature purposes, finer particle cement was used. In this test, a dry blend of each material—API Class C cement, API Class G cement, and normalized granite—is evaluated. A PSD measurement instrument using laser diffraction is used for analyzing the dry powder of each material.

Viscous Properties. A scientific rheometer was used instead of a rotational viscometer to measure the rheology of the slurry due to the capability of cooling down the temperature below room temperature in the rheometer. A scientific rheometer also has the benefit of having the ability to measure shear stress at a very low shear rate (0.01 s^{-1}), leading to a better yield stress estimation. Before testing, each sample was premixed and conditioned for 30 minutes at 4°C, 15°C, and 25°C in an atmospheric consistometer. The rheometer was conditioned for each temperature before the test to avoid temperature shock during the testing. The test program follows the API RP 10B-2 standard, where the fluid was subjected to a ramp up shear rate, followed by a ramp-down shear rate. Shear rates ranging from 0.01 to 511 s^{-1} were applied to the slurry.

Pumpability and Consistency. A pressurized consistometer, specified in API RP 10B-2, was used to evaluate the workability and setting time of each slurry under examination at targeted temperatures with a pressure of 124 bar. Before the experiment, the equipment was conditioned at the specified temperature and controlled with a cooling bath attachment. Pressure was ramped up for approximately 10 minutes to achieve the target pressure of 124 bar. Pumpability was measured from the starting point up to 80 Bc, and the pumping time is the total time measured at 70 Bc.

Static Fluid Loss. The double-ended fluid-loss cell was used to assess the performance of each slurry, as per the API RP 10B-2 standard (API RP 10B-2 2013). To conduct the test, the slurry is mixed and conditioned for 30 minutes, after which it is poured into the cells. Because the equipment does not have temperature control, the test is carried out only at room temperature (approximately 22°C). The slurry is then poured into the cell, and the 325 mesh is placed, and will be in contact with slurry. The cell is then pressurized to the targeted pressure of 124 bar, and the filtrate is measured until either 30 minutes have passed or the gas blows dry.

Static Gel Strength. Static gel strength refers to the yield stress developed by cement during the reaction process, which increases with time due to hydration. During the transition of cement from liquid to solid, it loses its hydrostatic pressure, which may cause gas to flow through the cement column (Al-Buraik et al. 1998). To meet industry standards, the acceptable duration for gas transition should not exceed 45 minutes. A static gel strength test is performed in accordance with API RP 10B-6 (2010) using a mechanical gel strength machine to measure the development of static gel strength in cement at different temperatures. The equipment is an addition to the ultrasonic cement analyzer and includes a mechanical rotation assembly. This assembly transfers the rotation from the motor located at the cap to the paddle inside the slurry chamber. The machine can generate small shear forces, and the resistance produced is measured and converted into a static gel strength. To conduct the test, the sample is conditioned at the desired temperature and pressure, followed by periodic mechanical rotations at 0.01 rev/min for 1 minute, with a resting time of 10 minutes between each cycle. The transition time is defined as the period during which the slurry develops strength from 50 Pa (100 lb/100 ft^2) to 250 Pa (500 lb/100 ft^2). A static gel strength of 250 Pa (500 lb/100 ft^2) indicates adequate internal strength in cement to withstand gas attacks, according to Sabins et al. (1982).

Compressive Strength. The slurries were cured in a cylindrical mold (51-mm diameter and 90-mm length) and placed inside a pressurized chamber and water bath to control the temperature for 1 day, 3 days, and 7 days of curing time. Temperatures of 4°C, 15°C, and 25°C were selected to better represent the shallow-depth cementing in the North Sea area. The curing pressure was 124 bar for all samples. The cured cement samples were removed from the mold, prepared, and placed in a hydraulic compression machine. The test records the maximum compressive strength of the material before deformation. A minimum of three tests were performed for each measurement to ensure the reliability of the measurement. Referring to the industry practices, a minimum compressive strength of 500 psi or 3.4 MPa is required for continuing the drilling process for the next sections.

X-Ray Diffraction. XRD analyses were done to observe the changes in the mineral content of the cementitious material at different temperatures. The Bruker-AXS Micro-diffractometer D8 Advance, which uses CuKα radiation (40.0 kV, 25.0 mA), was used to observe phase changes of each material. The diffractometer had a 2θ range from 5° to 90°, with a 1°/minute step and 0.010° increment. Before testing, the samples were manually ground and dried in a vacuum oven for 24 hours.

Result and Discussion

Dry Precursor Characterization. The dry solid precursor of each cementitious material was first evaluated to better understand the underlying compounds of each phase before their reaction. The XRD results in **Fig. 1** characterize the distinct properties of each material. Portland-based cement API Classes G and C exhibit typical cement phases such as alite (C_3S), belite, C_3A, and C_4AF, with different peaks corresponding to different phases. Notably, the higher C_3A content in Class C cement contributes to faster reaction times and higher early strength development compared to that of the API Class G cement (Quennoz 2011).

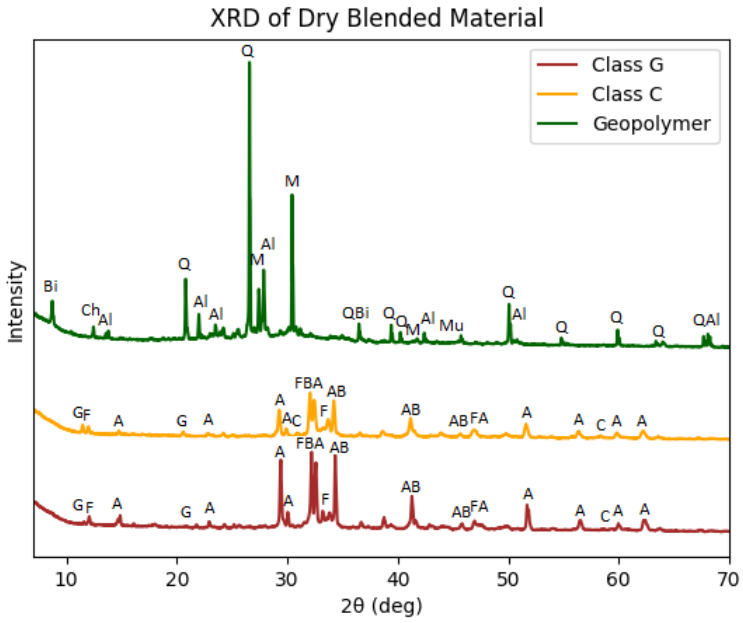

Fig. 1—XRD results of dry blended material Class G (red), Class C (yellow), geopolymer (green). A: alite, Al: albite, B: belite, Bi: biotite, C: C_3A, Ch: chamosite, F: C_4AF, G: gypsum, M: microcline, Mu: muscovite, Q: quartz.

The XRD results also show the difference in composition of the applied geopolymer compared to the Portland-based cement. The geopolymer shows higher crystallinity and higher intensity peaks with completely different phases than cement. The XRD results confirm the composition of minerals such as quartz, albite, microcline, and biotite that dominates the precursor phase of geopolymer precursors. Quartz is the most dominant mineral shown in XRD and mostly present from granite. Other minerals contributing to the mixture are microcline, an alkali feldspar, albite in plagioclase feldspar, and biotite. Due to high amorphous content, BFS presence is unable to be observed in this XRD of the mixture. BFS confirmation in XRD can be confirmed as a small hump around 30 2θ degrees.

To gain further insight into the reactivity of each material, PSD analysis was conducted on all solid precursors, as shown in **Fig. 2.** The PSD results demonstrate several particle-size differences, with Portland Class C cement exhibiting the finest particles, with an average particle size of 11.85 µm, compared with Class G cement with an average particle size of 30.19 µm. Granite, the main geopolymer precursor, shows larger particle sizes, with an average of 107.42 µm. Larger particle sizes typically result in lower material reactivity, requiring the use of BFS to normalize granite's performance for early strength development. The reactivity of cementitious materials is particularly critical when working with low temperatures and low pore pressure conditions, as the low-reactivity material is unlikely to react. Therefore, mechanical activation through particle-size optimization can have a significant impact on cementitious material performance, especially for geopolymer's precursor (Zerzouri et al. 2022). Additionally, particle size affects the slurry density due to its influence on water consumption. Smaller particle sizes can handle a higher percentage of water, leading to a lower slurry density. **Table 3** provides a summary of measurements such as density and particle size. It indicates that both Class C cements (rapid-hardening and gas tight cement) can yield a final slurry density of 1.60 and 1.66 SG, measured by pressurized mud balance. In contrast, Class G cement and geopolymer, with larger particle sizes, exhibit a higher slurry density of 1.89 SG.

Rheology. Flow curve results (shear rate vs. shear stress) at different temperatures are presented in **Fig. 3.** The profile is presented in both ramp up and ramp-down measurements. In general, the kinetic energy of the particles increases with temperature, leading to lower viscosity in most cases. However, the viscosity of cementitious material is influenced by various factors such as particle size, water content, surface chemistry of particles, chemical reaction, shear history, and temperature. From the result, it can be observed that rapid-hardening cement is only slightly affected by temperatures ranging from 4 to 25°C; even though rapid-hardening cement has a smaller particle size, it is mixed with a huge amount of water, reaching 85%, which seems to dominate its rheological behavior. Similarly, the applied gas tight cement also uses based cement Class C mixed with less water percentage for about 65%. It exhibits unique behavior on the ramp up and ramp down, which shows a higher degree of thixotropy and is more sensitive to temperature. Moreover, the maximum peak of shear stress at a low shear rate indicates gelation due to the surface chemistry of particles, which is the effect of colloidal silica

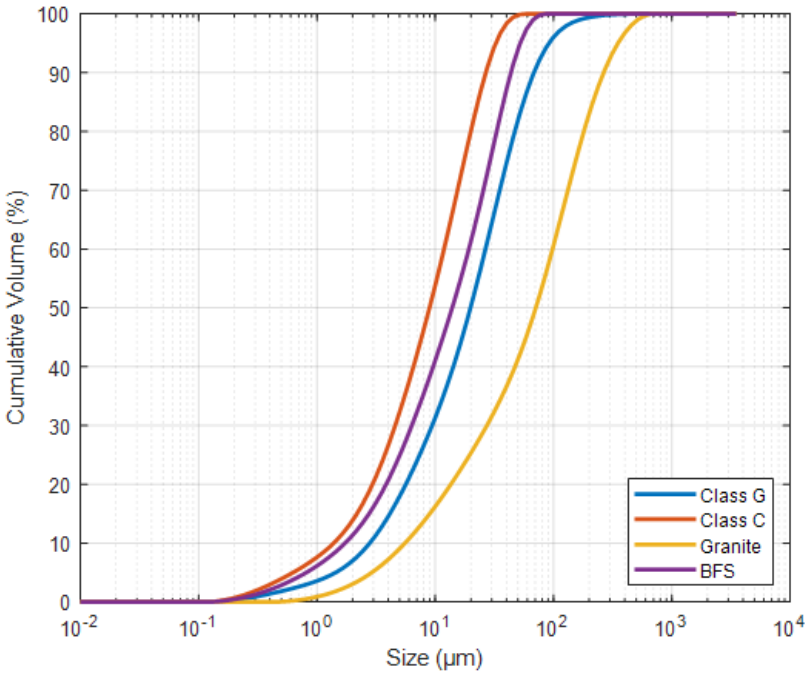

Fig. 2—PSD of solid precursor Portland cement Class C (red) and Class G (blue) and granite-based geopolymer (yellow) and BFS (purple).

Cementitious Material	Measured Density	PSD		Setting Time 70 Bc (h:mm)		Yield Stress (Pa)			SGS Transition Time (h:mm)		
		Avg (μm)	D90/D10	15°C	25°C	4°C	15°C	25°C	4°C	15°C	25°C
Neat G cement	1.89	30.19	24.44	8:27	5:06	11.389	10.838	19.928	03:59	1:55	00:56
Rapid-hardening cement	1.60	11.85	19.34	5:25	2:14	12.098	17.101	18.775	03:18	0:52	00:25
Gas tight cement	1.66	11.85	19.34	4:47	3:19	8.054	11.029	19.083	06:47	2:22	00:59
Granite-based geopolymer	1.89	107.42	47.83	8:37	4:42	16.384	15.151	15.824	18:21	5:15	00:52

Table 3—Test result summary.

additive (Senff et al. 2009). Neat API Class G cement has a coarser particle size than Class C cement; however, the temperature trend is comparable with gas tight cement with higher viscosity at 25°C due to possible effects of reaction. Geopolymer is significantly affected by temperature, following the typical trend. It has a larger particle size, which is less reactive; therefore, the rheological behavior is likely to be more dominated by kinetic energy and particle collisions. The geopolymer slurry shows high viscosity at low temperatures. In this case, it also shows high viscosity at higher shear rates.

Yield stress estimation was performed on the flow curve chart by using linear extrapolation. Zamora and Power (2002) extrapolated the results measured at the shear stress at 3 rev/min and 6 rev/min, using Eq. 1:

$$\tau_y = 2\tau_3 + \tau_6, \quad (1)$$

with τ_y as yield stress, τ_3 as shear stress at 3 rev/min reading, and τ_6 as shear stress at 6 rev/min reading. Adopting a similar concept of extrapolation was performed on stable regions outside of gel effect, such as those present in gas tight cement (Agista et al. 2022b). The result is presented in **Table 3** for each material at different temperatures. One needs to emphasize here that the yield stress estimated through the flow curve is a type of dynamic yield stress (Qian and Kawashima 2018). Moreover, as time-dependent material, the property of cementitious material changes over time, which means the viscosity will change with longer time. Therefore, measurement of the slurry over a certain time until it changes the phase, such as a consistency test, is necessary to be performed.

Pumpability and Consistency. Pumpability tests are performed using the pressurized consistometer to measure the restriction torque of rotation. A paddle is inserted into the consistometer cylinder, which is rotated at 150 rev/min. This test evaluates the thickening of cementitious material over time until it becomes too thick to be pumpable. To differentiate between the consistency and setting time of materials, it is important to understand that setting time refers to the time it takes for the material to harden from a gel state, while thickening time, also known as pumpability/workability time, is the amount of time the slurry remains in the fluid phase before gelation occurs. The test mimics the continuous shear experienced by the slurry during the actual pumping process. There are varied values of the limit in pumpability depending on the operator such as 40 or 70 Bc. Beyond this set limit, the slurries are considered to be unpumpable.

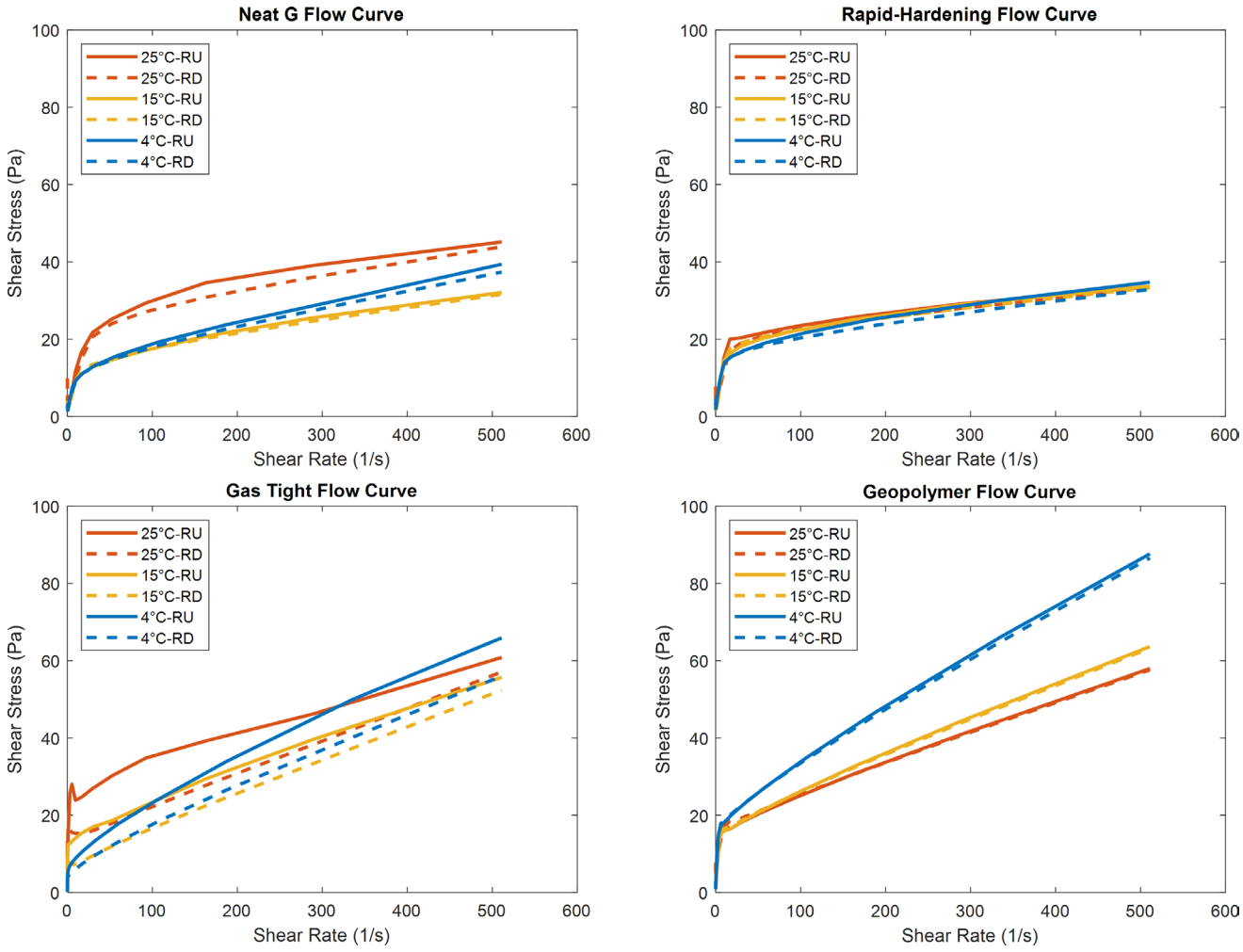

Fig. 3—Flow curve results of neat G (upper left), rapid-hardening (upper right), gas tight (lower left), and geopolymer (lower right). The solid line represents ramp up test, and the dashed line represents ramp-down test.

Fig. 4 illustrates the results for tests at 15°C and 25°C, while tests at 4°C were not available due to limitations with the equipment and cooling source, as well as concerns related to the exothermic reaction caused by the slurries. The results indicate that all materials experienced delayed thickening at lower temperatures. Also, both rapid-hardening and gas tight cements have the fastest thickening time at lower temperatures, indicating a faster reaction due to their fine particles and different composition. Gas tight cement exhibits better performance for low temperatures showing the right-angle set trend, which is useful for cementing at flow zones. Both neat G and geopolymer have comparable thickening time at both temperatures, and the only difference observed is that at 25°C, neat G cement has higher initial consistency.

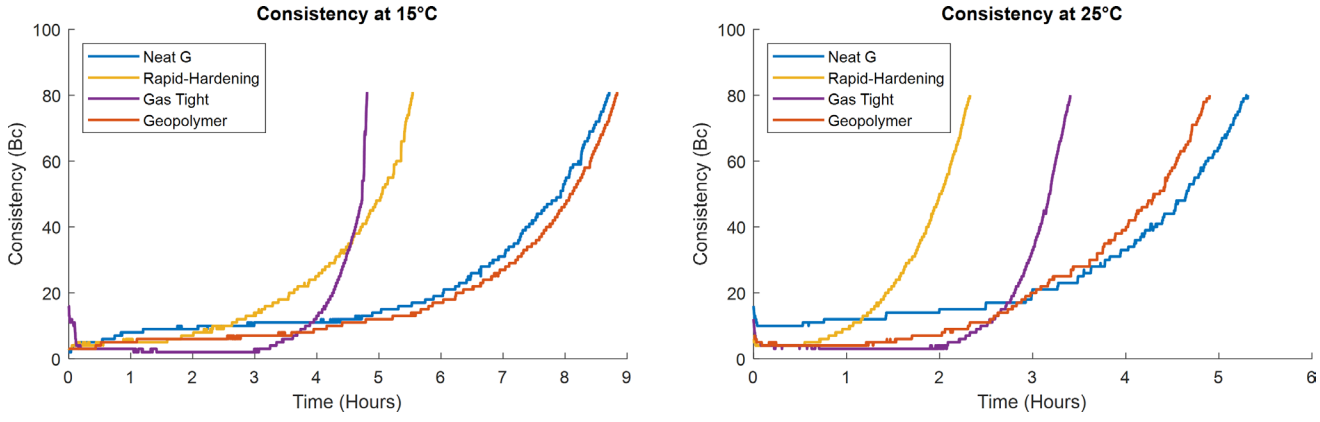

Fig. 4—Pumpability and consistency test at 15°C (left) and 25°C (right).

Static Gel Strength. The measurement of static gel strength is commonly used to assess the transition of cementitious materials from a slurry to a solid state. This test is designed to simulate the development of gel strength after the slurry is placed into a wellbore. The measurements are performed to evaluate the gel strength after a period of static conditions. The machine conducts a rotational test that measures the restriction every 10 minutes during a measurement time of 1 minute. The concept of static gel strength was introduced to address short-term gas migration. The test measures the time slurry takes for the transition from 50 to 250 Pa, which is known as the critical static gel strength period. At 50 Pa, the slurry is believed to have lost significant hydrostatic pressure due to reactions but is weak enough to be attacked by gas, while at 250 Pa, the slurry is believed to have enough gel strength to counter gas invasion. According to industry practices, a transition time of less than 45 minutes is required to handle gas migration (DeBruijn and Whitton 2021).

In this study, static gel strengths were measured mechanically for the four cementitious materials at three different temperatures. The results of the static gel strength profile are presented in **Fig. 5**, and the transition times are presented in **Table 3**. A similar trend of prolonged gel strength development at lower temperatures was observed for all materials. However, some materials, such as the geopolymer, were more sensitive to temperature due to their nature. Geopolymers require more energy to dissolve and activate geopolymerization reaction at lower temperatures. On the other hand, Portland-based cement also showed prolonged effects due to temperature. In the case of gas tight and rapid-hardening cements, both had a fast transition time at 25°C but significantly prolonged gelation at a low temperature of 4°C. Similar behavior was observed in the neat G cement, which had the fastest transition time at 4°C of all cement types. Temperature significantly affects gel strength development, as it mostly contributes to the hydration reaction or geopolymerization of cementitious materials. Considering offshore Norway, this experiment indicates that the upper parts of the cementing section might be more prone to gas attack due to prolonged gel strength development and longer transition time.

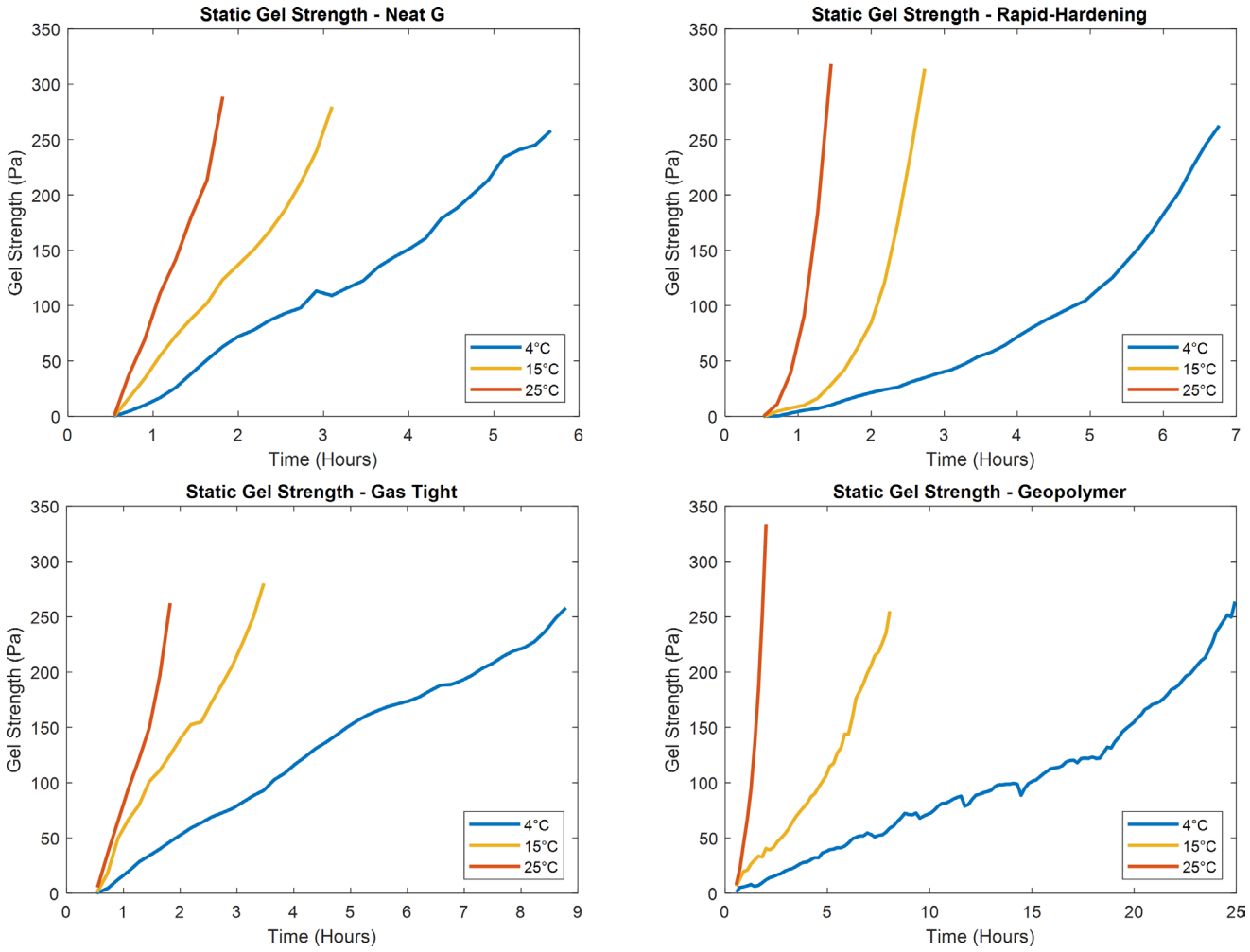

Fig. 5—Static gel strength of neat G cement (upper left), rapid-hardening cement (upper right), gas tight cement (lower left), and the geopolymer (lower right).

Compressive Strength. The early compressive strength of materials was measured under various conditions for 1 day, 3 days, and 7 days of curing. To simulate downhole conditions, a pressurized cell with temperature control was used to cure each sample at a pressure of 124 bar and temperatures of 4°C, 15°C, and 25°C. Some pretreatments of the samples before testing, such as cutting and flattening the top and bottom of the cured samples, were performed. A correction factor was added to the measured compressive strength due to the varied length-to-diameter ratio following API TR 10TR7 (2017). This correction was essential to correct the overestimation of strength due to length-to-diameter ratios of less than 2. During the tests, a minimum of three specimens were tested to understand the measurement error and reproducibility. The average result is presented in **Fig. 6,** along with the standard deviation of the measurement. It is noticeable that some materials, such as the geopolymer and the neat API Class G cement, have lower standard deviations, while both rapid-hardening and gas tight cements exhibit higher standard deviations. Both types of cement use a water-extended system to lower the density, which

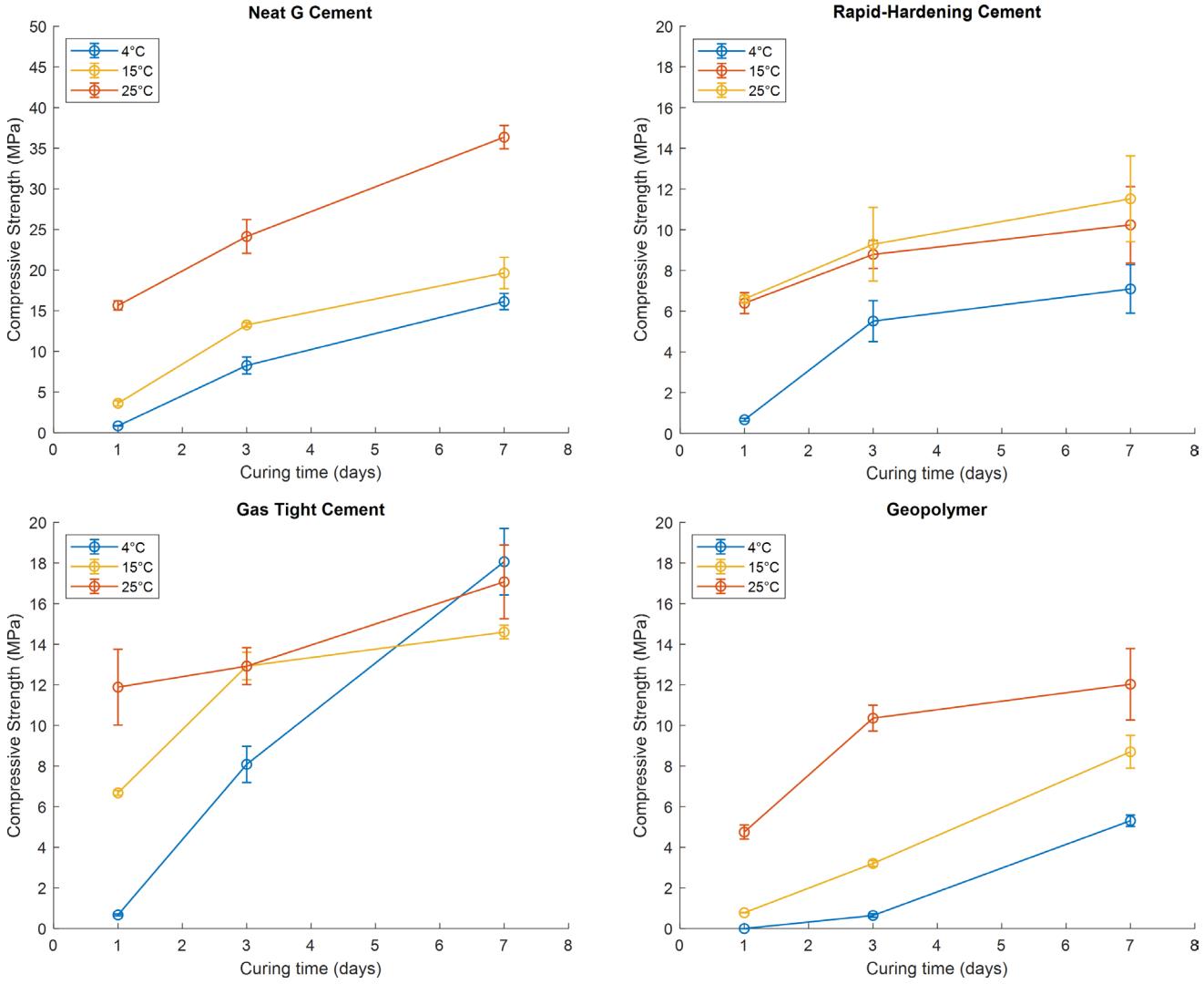

Fig. 6—Compressive test result of the four different cementitious materials. (Note that the scale of the measurements with neat G cement differs from the scale of the other measurements.)

could lead to some material deposition that occurs rapidly after mixing, conditioning, and placement of the samples in the curing mold. These events create slight differences in density, affecting the cured samples' strength.

The compressive strength shows a significant effect of temperature and time on the strength development. The neat G cement shows a predictable trend in the temperature and time effect on strength development. A unique behavior is observed for both rapid-hardening and gas tight cements. Rapid-hardening cement exhibits only slight differences in compressive strength at 15°C and 25°C for 1 and 2 days, while gas tight cement shows higher 7-day strength at the lower 4°C temperature. This anomaly could be explained by the effect of colloidal silica additives. A similar test on colloidal silica additives performed by Bu et al. (2018) at 4°C concluded that colloidal silica can retard cement initial hydration at low temperatures by absorbing Ca^{2+}, which then accelerates by promoting rapid reaction due to its reactivity. They also found out through XRD analysis and Fourier-transform infrared spectroscopy analysis that at 4°C consumption of $Ca(OH)_2$ to create C-S-H gels decreases, which could explain lower compressive strength initially while having constant increases of strength over time. Moreover, geopolymer shows late strength development at short-term periods, especially at low temperatures. However, at 25°C, it does show comparable strength with rapid-hardening cement.

To better observe the strength development of each material, an ultrasonic compressive strength analyzer was used. The equipment measured the transit time of the sonic sound traveling through the sample inside a pressurized chamber at different temperatures. The transit time was then correlated using average compressive strength data. The results are presented in three different graphs for each temperature profile in **Fig. 7.** The strength development behavior of each material can be observed over time. At 4°C, the rapid-hardening cement is the fastest material to develop strength within 1 day, while other materials take 2 or 3 days to harden. However, the final strength of the rapid-hardening cement is relatively lower compared with the gas tight and neat G cements. Considering the density difference, the gas tight cement shows comparable results with the neat G cement. Moreover, the behavior at 15°C shows that both rapid-hardening and gas tight cements harden faster compared with the material, indicating that both Class C-based cements are able to perform well at this temperature. At 25°C, all materials were able to harden to the required strength in less than 1 day.

Young's moduli were obtained using hydraulic crushing tests. The data are presented in **Fig. 8.** The geopolymer was not able to develop strength at low temperatures, and therefore, Young's modulus for this material is zero for the 1-day test. In general, the geopolymer also showed a lower Young's modulus, indicating higher flexibility of the material compared to other Portland-based cements. Kamali et al. (2021) observed similar behavior on the flexibility of their granite-based geopolymers. A normal trend of Young's modulus with

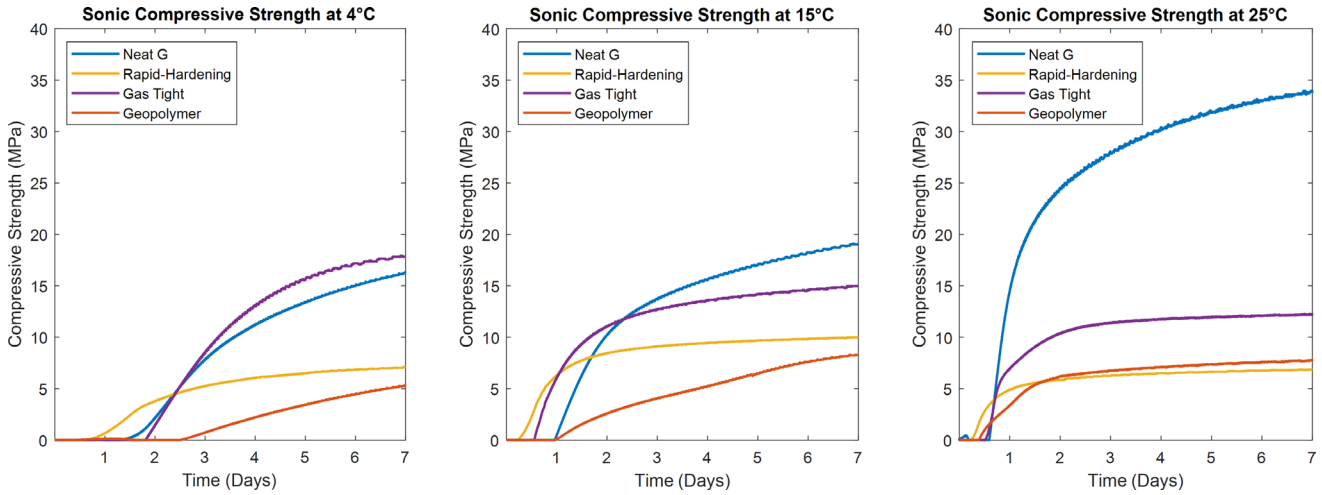

Fig. 7—Sonic strength development measured at three different temperatures for four different cementitious materials.

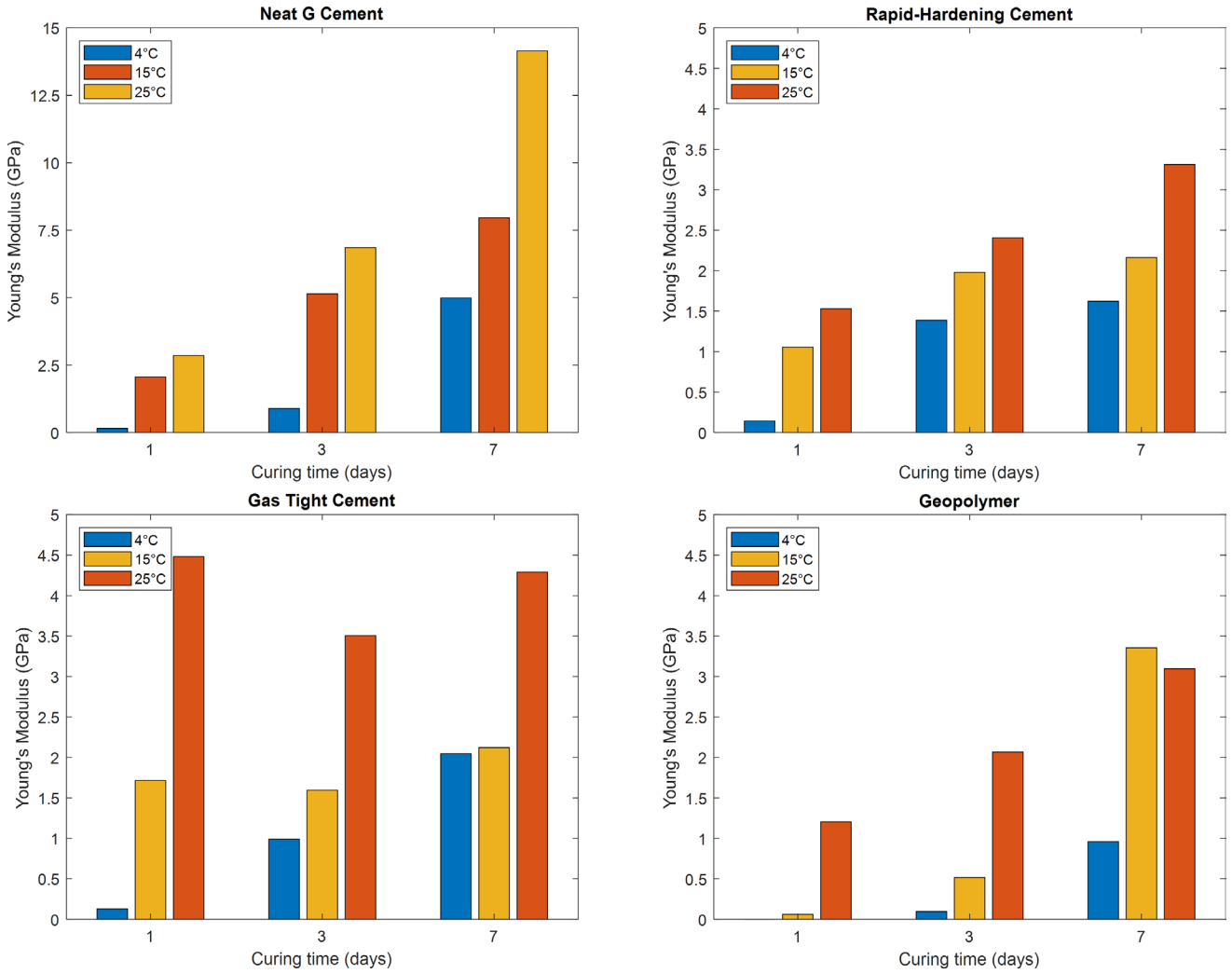

Fig. 8—Young's modulus of four different cementitious materials. (Note that the scale of the measurements with API Class G cement differs from the scale of the other measurements.)

respect to curing days and temperature was observed for both the neat API Class G and the rapid-hardening cements. However, a unique behavior of gas tight cement was observed due to the effect of colloidal silica additives, as explained previously.

X-Ray Diffraction. XRD tests were used to further evaluate and confirm the behavior of each cementitious material. The 1-day and 7-day samples, which were cured under different temperatures, were then prepared and dried before the XRD test. The temperature is known to affect the hydration kinetics of the cement, resulting in different phases being consumed and different hydration products being produced. This could provide further explanation for the different strength development observed in the previous results.

The dry precursor XRD of the neat G cement is shown in **Fig. 1**, which is mostly dominated by the C_3S (alite) and C_2S (belite) phases. The XRD results of the neat G cement cured at different temperatures for 1 day and 7 days are presented in **Fig. 9.** It can be observed that the higher temperature for 1-day curing yielded a higher amount of Portlandite as one of the major hydration products. It can also be seen that ettringite, which is normally present during the early stages of cement reaction, is present. The XRD results also confirm the consumption of precursor phases of Portland cement, such as C_3S and C_2S. Lower temperatures showed a higher presence of C_3S and C_2S, indicating less consumption of the precursors. Moreover, the 7-day results showed a further increase in Portlandite and the disappearance of ettringite, which explains the increase in material strength.

Fig. 10 shows a similar trend and behavior for the rapid-hardening cement. However, different intensity peaks are observed, which account for a rich chloride AFm phase resembling a hydrocalumite-like structure. The presence of this phase in the rapid hardening cement is due to the use of seawater. The intensity of these peaks increases with higher temperatures and longer curing time. Additionally, the XRD results of the gas tight cement in **Fig. 11** show a similar trend with temperature and pressure. However, the XRD result reveals a high amorphous behavior of the material, which is noticeable from the lower peak of Portlandite and a higher hump in the baseline due to the interference of the amorphous content of the material.

The XRD analysis of the geopolymer in **Fig. 12** shows a significantly different result compared to the Portland-based cement presented above. Previous studies on a similar granite-based geopolymer showed that quartz was the major phase followed by albite and microcline (Omran and Khalifeh 2022; Chamssine et al. 2022; Khalifeh et al. 2016). The intensity analysis of the geopolymer XRD result shows a reduction in precursor phases such as albite and microcline at different temperatures and curing times. Higher quartz intensity is observed in the longer 7-day curing period compared with the 1-day curing period, indicating the consumption of albite and microcline during geopolymerization, which were initially present in the dry solid precursor. However, the current understanding of the geopolymer product phase is limited, and further studies are required for deeper insights.

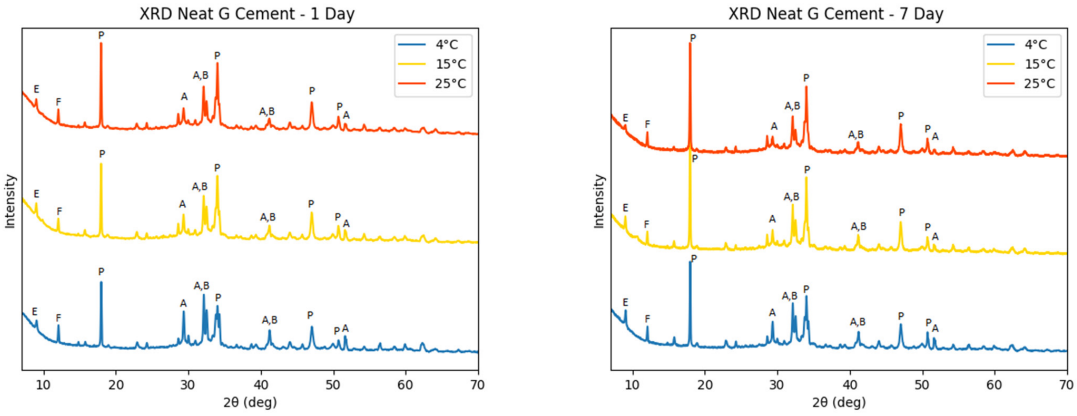

Fig. 9—XRD results of neat G cement cured for 1 day and 7 days at temperatures of 4°C, 15°C, and 25°C. A: alite, Br: brownmillerite, E: ettringite, F: C_4AF, P: Portlandite.

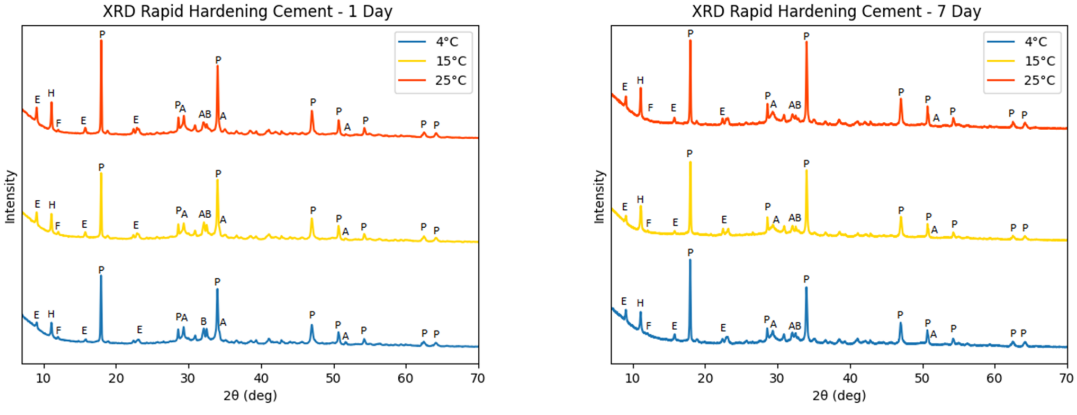

Fig. 10—XRD results of rapid-hardening cement cured for 1 day and 7 days at temperatures of 4°C, 15°C, and 25°C. A: alite, B, belite, E: ettringite, F: C_4AF, H: hydrocalumite, P: Portlandite.

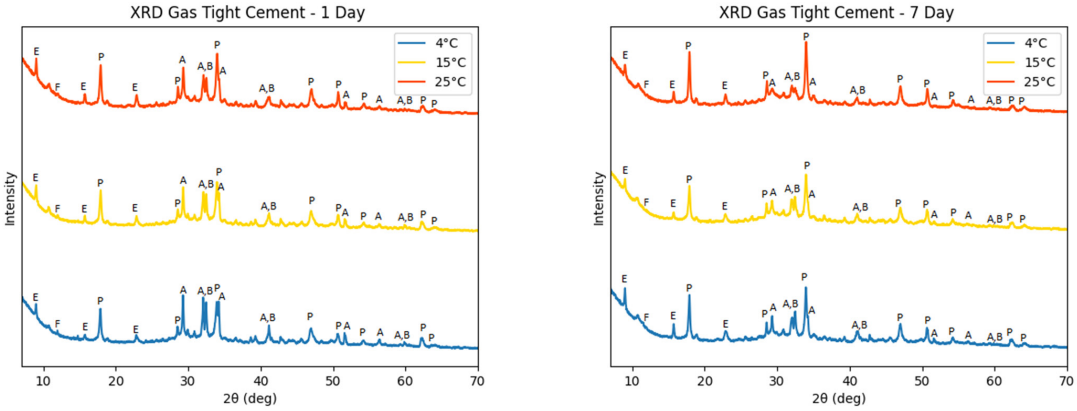

Fig. 11—XRD results of gas tight cement cured for 1 day and 7 days at temperatures of 4°C, 15°C, and 25°C. A: alite, B, belite, E: ettringite, F: C_4AF, P: Portlandite.

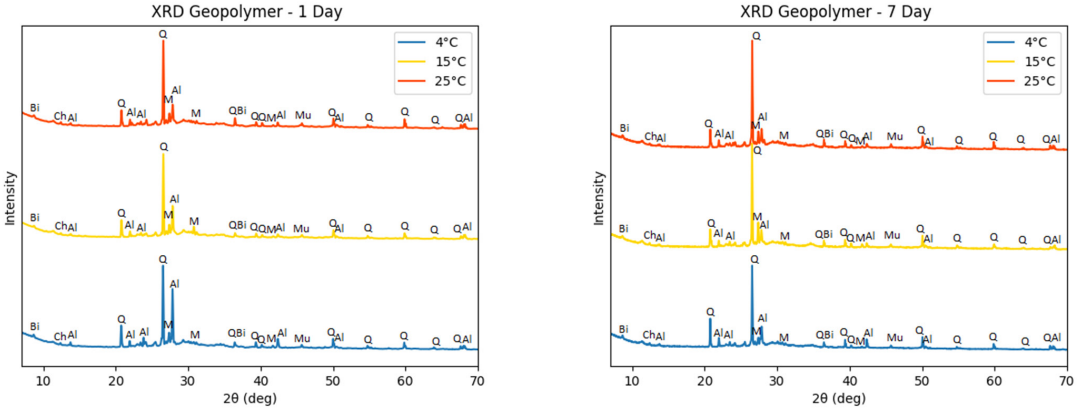

Fig. 12—XRD results of the geopolymer cured for 1 day and 7 days at temperatures of 4°C, 15, and 25°C. Al: albite, Bi: biotite, Ch: chamosite, M: microcline, Mu: muscovite, Q: quartz.

Conclusion

Early fluid-state and solid-state performances of four cementitious materials, namely, neat G cement, rapid-hardening cement, gas tight cement, and normalized granite-based geopolymer, are presented showing their suitability in low-temperature shallow-depth cementing applications. The results show that the performance of each material in terms of rheology, pumpability, static gel strength, and compressive strength is significantly affected by temperature and curing time. Reducing temperature increases the viscosity of the geopolymer at lower temperatures, while the neat G cement shows higher viscosity with increasing temperature. Temperature less significantly affects the viscosity of rapid-hardening and gas tight cements. Lower temperatures result in delayed hydration and geopolymerization reactions, leading to prolonged pumpability, static gel strength, and lower strength development. This could introduce the risk of fluid invasion when the system is still in fluid state. XRD analysis was performed to confirm the consumption of dry precursors and the product of hydration and geopolymerization phases with varied temperatures and curing time, which drove different reaction kinetics.

The challenges of achieving sufficient strength in low-temperature zones and the importance of waiting-on-cement periods or incorporating strength enhancement additives to ensure long-term well integrity are highlighted in this paper. The results demonstrate that the performances such as curing time of cementitious materials are highly dependent on temperature. These findings can inform the development and optimization of cementitious materials for low-temperature shallow-depth applications. Further research is necessary to gain a deeper understanding of the geopolymerization reaction and the resulting phases in the geopolymer product.

Acknowledgments

The authors acknowledge the Research Council of Norway (RCN) for financing the Centre for Research-based Innovation "SWIPA—Centre for Subsurface Well Integrity, Plugging and Abandonment," RCN proj. no. 309646, for which the work has been carried out. The center is also financed by the operating companies AkerBP, Equinor ASA, and Wintershall Dea Norway and includes in addition more than 20 in-kind contributing industry partners. The R&D partners in SWIPA are SINTEF, NORCE, IFE, NTNU, and UiS. The authors also gratefully acknowledge Halliburton and Gunnar Lende for their technical support and input.

References

Agista, M. N., Khalifeh, M., and Saasen, A. 2022a. Evaluation of Zonal Isolation Material for Low Temperature Shallow Gas Zone Application. Paper presented at the SPE Asia Pacific Oil & Gas Conference and Exhibition, Adelaide, Australia, 17–19 October. SPE-210751-MS. https://doi.org/10.2118/210751-MS.

Agista, M. N., Khalifeh, M., and Saasen, A. 2022b. In-Depth Rheological Evaluation of Gas Tight Cement for Shallow Gas Application. Paper presented at the SPE Asia Pacific Oil & Gas Conference and Exhibition, Adelaide, Australia, 17–19 October. SPE-210705-MS. https://doi.org/10.2118/210705-MS.

Al-Buraik, K., Al-Abdulqader, K., and Bsaibes, R. 1998. Prevention of Shallow Gas Migration Through Cement. Paper presented at the IADC/SPE Asia Pacific Drilling Technology, Jakarta, Indonesia, 7–9 September. SPE-47775-MS. https://doi.org/10.2118/47775-MS.

Al Ramadan, M., Salehi, S., Kwatia, G. et al. 2019. Experimental Investigation of Well Integrity: Annular Gas Migration in Cement Column. *J Pet Sci Eng* **179**: 126–135. https://doi.org/10.1016/j.petrol.2019.04.023.

API RP 10B-2, *Recommended Practice for Testing Well Cements*. 2013. Washington, DC, USA: American Petroleum Institute (API).

API RP 10B-6, *Recommended Practice on Determining the Static Gel Strength of Cement Formulations*. 2010. Washington, DC, USA: American Petroleum Institute (API).

API TR 10TR7, *Mechanical Behavior of Cement*. 2017. Washington, DC, USA: American Petroleum Institute (API).

Bachu, S. 2017. Analysis of Gas Leakage Occurrence along Wells in Alberta, Canada, from A GHG Perspective – Gas Migration Outside Well Casing. *Int J Greenh Gas Control* **61**: 146–154. https://doi.org/10.1016/j.ijggc.2017.04.003.

Bensted, J. 1991. API Class C Rapid-Hardening Oilwell Cement. *World Cement* **22**.

Bentz, D. P., Garboczi, E. J., Haecker, C. J. et al. 1999. Effects of Cement Particle Size Distribution on Performance Properties of Portland Cement-Based Materials. *Cem Concr Res* **29** (10): 1663–1671. https://doi.org/10.1016/S0008-8846(99)00163-5.

Bjordal, A., Harris, K. L., and Olaussen, S. R. 1993. Colloidal Silica Cement: Description and Use in North Sea Operations. Paper presented at the Offshore Europe, Aberdeen, United Kingdom, 7–10 September. SPE-26725-MS. https://doi.org/10.2118/26725-MS.

Böttner, C., Haeckel, M., Schmidt, M. et al. 2020. Greenhouse Gas Emissions from Marine Decommissioned Hydrocarbon Wells: Leakage Detection, Monitoring and Mitigation Strategies. *Int J Greenh Gas Control* **100**: 103119. https://doi.org/10.1016/j.ijggc.2020.103119.

Bu, Y., Hou, X., Wang, C. et al. 2018. Effect of Colloidal Nanosilica on Early-Age Compressive Strength of Oil Well Cement Stone at Low Temperature. *Constr Build Mater* **171**: 690–696. https://doi.org/10.1016/j.conbuildmat.2018.03.220.

Chamssine, F., Khalifeh, M., Eid, E. et al. 2021. Effects of Temperature and Chemical Admixtures on the Properties of Rock-Based Geopolymers Designed for Zonal Isolation and Well Abandonment. Paper presented at the ASME 2021 40th International Conference on Ocean, Offshore and Arctic Engineering, Virtual, Online, 21–30 June. OMAE2021-60808. https://doi.org/10.1115/OMAE2021-60808.

Chamssine, F., Khalifeh, M., and Saasen, A. 2022. Effect of Zn2+ and K+ as Retarding Agents on Rock-Based Geopolymers for Downhole Cementing Operations. *J Energy Resour Technol* **144** (5): 5. https://doi.org/10.1115/1.4053710.

Davidovits, J. 2005. Geopolymer, Green Chemistry and Sustainable Development Solutions. Paper presented at the Proceedings of the World Congress Geopolymer 2005.

Davidovits, J. 2020. *Geopolymer Chemistry and Applications*, 5th edition. Saint-Quentin: Geopolymer Institute.

DeBruijn, G. and Whitton, S. M. 2021. Fluids. In *In Applied Well Cementing Engineering*, 163–251. Amsterdam, Netherlands: Elsevier.

Drecq, P. and Parcevaux, P. A. 1988. A Single Technique Solves Gas Migration Problems Across A Wide Range of Conditions. Paper presented at the International Meeting on Petroleum Engineering, Tianjin, China, 1–4 November. SPE-17629-MS. https://doi.org/10.2118/17629-MS.

Gomado, F. D., Khalifeh, M., and Aasen, J. A. 2023. Expandable Geopolymers for Improved Zonal Isolation and Plugging. Paper presented at the SPE/IADC International Drilling Conference and Exhibition, Stavanger, Norway, 7–9 March. SPE-212493-MS. https://doi.org/10.2118/212493-MS.

Grinrod, M., Vassoy, B., and Dingsoyr, E. O. 1988. Development and Use of a Gas-Tight Cement. Paper presented at the IADC/SPE Drilling Conference, Dallas, Texas, USA, 28 February. SPE-17258-MS. https://doi.org/10.2118/17258-MS.

Hewlett, P. and Liska, M. 2019. *Lea's Chemistry of Cement and Concrete*. Oxford, United Kingdom: Butterworth-Heinemann.

Kamali, M., Khalifeh, M., Saasen, A. et al. 2021. Alternative Setting Materials for Primary Cementing and Zonal Isolation – Laboratory Evaluation of Rheological and Mechanical Properties. *J Pet Sci Eng* **201**: 108455. https://doi.org/10.1016/j.petrol.2021.108455.

Khalifeh, M., Delabroy, L., and Kverneland, J. 2023. Potential Utilization of Rock-Based Geopolymers for Oil Well Cementing at Cold Areas. Paper presented at the SPE/IADC International Drilling Conference and Exhibition, Stavanger, Norway, 7–9 March. SPE-212442-MS. https://doi.org/10.2118/212442-MS.

Khalifeh, M., Saasen, A., Hodne, H. et al. 2019. Laboratory Evaluation of Rock-Based Geopolymers for Zonal Isolation and Permanent P&A Applications. *J Pet Sci Eng* **175**: 352–362. https://doi.org/10.1016/j.petrol.2018.12.065.

Khalifeh, M., Saasen, A., Vrålstad, T. et al. 2016. Experimental Study on the Synthesis and Characterization of Aplite Rock-Based Geopolymers. *J Sustain Cem* **5** (4): 233–246. https://doi.org/10.1080/21650373.2015.1044049.

Nelson, E. B. and Guillot, D. 2006. *Well Cementing*, 773. https://doi.org/10.4088/jcp.v67n1209.

NORSOK Standard D-010, *Well Integrity in Drilling and Well Operations*. 2013. Lysaker, Norway: Standards Norway.

Omran, M. and Khalifeh, M. 2022. Development of Low Carbon Dioxide Intensive Rock-Based Geopolymers for Well Cementing Applications – One-Part Geopolymer. Paper presented at the ASME 2022 41st International Conference on Ocean, Offshore and Arctic Engineering, Hamburg, Germany, 5–10 June. OMAE2022-78535. https://doi.org/10.1115/OMAE2022-78535.

Omran, M., Khalifeh, M., and Saasen, A. 2022. Influence of Activators and Admixtures on Rheology of Geopolymer Slurries for Well Cementing Applications. Paper presented at the SPE Asia Pacific Oil & Gas Conference and Exhibition, Adelaide, Australia, 17–19 October. SPE-210698-MS. https://doi.org/10.2118/210698-MS.

Opseth, T. L., Ribesen, B. T., Syrstad, B. et al. 2009. Curing Shallow Water Flow in a North Sea Exploration Well Exposed to Shallow Gas. Paper presented at the SPE Offshore Europe Oil and Gas Conference and Exhibition, Aberdeen, UK, 8–11 September. SPE-124607-MS. https://doi.org/10.2118/124607-MS.

Qian, Y. and Kawashima, S. 2018. Distinguishing Dynamic and Static Yield Stress of Fresh Cement Mortars through Thixotropy. *Cem Concr Compos* **86**: 288–296. https://doi.org/10.1016/j.cemconcomp.2017.11.019.

Quennoz, A. 2011. *Hydration Of C3A With Calcium Sulfate Alone and in The Presence of Calcium Silicate*. Urban: EPFL.

Rae, P. and Di Lullo, G. 2004. Lightweight Cement Formulations for Deep Water Cementing: Fact and Fiction. Paper presented at the SPE Annual Technical Conference and Exhibition, Houston, Texas, USA, 26–29 September. SPE-91002-MS. https://doi.org/10.2118/91002-MS.

Sabins, F. L., Tinsley, J. M., and Sutton, D. L. 1982. Transition Time of Cement Slurries Between the Fluid and Set States. *SPE J.* **22** (6): 875–882. SPE-9285-PA. https://doi.org/10.2118/9285-PA.

Senff, L., Labrincha, J. A., Ferreira, V. M. et al. 2009. Effect of Nano-Silica on Rheology and Fresh Properties of Cement Pastes and Mortars. *Constr Build Mater* **23** (7): 2487–2491. https://doi.org/10.1016/j.conbuildmat.2009.02.005.

Smith, R. C. and Calvert, D. G. 1975. The Use of Sea Water in Well Cementing. *J Pet Technol* **27** (6): 759–764. SPE-5030-PA. https://doi.org/10.2118/5030-PA.

Tveit, M. R., Khalifeh, M., Nordam, T. et al. 2021. The Fate of Hydrocarbon Leaks from Plugged and Abandoned Wells by Means of Natural Seepages. *J Pet Sci Eng* **196**: 108004. https://doi.org/10.1016/j.petrol.2020.108004.

Vielstädte, L., Haeckel, M., Karstens, J. et al. 2017. Shallow Gas Migration along Hydrocarbon Wells-An Unconsidered, Anthropogenic Source of Biogenic Methane in the North Sea. *Environ Sci Technol* **51** (17): 10262–10268. https://doi.org/10.1021/acs.est.7b02732.

Wilpshaar, M, Bruin, G, Versteijlen, N et al. 2021. Comment on "Greenhouse Gas Emissions From Marine Decommissioned Hydrocarbon Wells: Leakage Detection, Monitoring and Mitigation Strategies" by Christoph Böttner, Matthias Haeckel, Mark Schmidt, Christian Berndt, Lisa Vielstädte, Jakob A. Kutsch, Jens Karstens & Tim Weiß.. *Int J Greenh Gas Control* **110**: 103119. https://doi.org/10.1016/j.ijggc.2020.103119.

Xu, Y., He, T., Yang, R. et al. 2023. New Insights into the Impact of Inorganic Salt on Cement Pastes Mixed with Alkali Free Liquid Accelerator in Low Temperature. *J Build Eng* **70**: 106419. https://doi.org/10.1016/j.jobe.2023.106419.

Zamora, M. and Power, D. 2002. Making a Case for AADE Hydraulics and the Unified Rheological Model. In *Drilling & Completion Fluids and Waste Management*, 1–8.

Zerzouri, M., Hamzaoui, R., Ziyani, L. et al. 2022. Influence of Slag Based Pre-Geopolymer Powders Obtained by Mechanosynthesis on Structure, Microstructure and Mechanical Performance of Geopolymer Pastes. *Constr Build Mater* **361**: 129637. https://doi.org/10.1016/j.conbuildmat.2022.129637.